Research on Chemical Intermediates (2018) 44:6569–6590
https://doi.org/10.1007/s11164-018-3509-7

Synthesis of flower-like Bi_2O_4/ZnO heterojunction and mechanism of enhanced photodegradation for organic contaminants under visible light

Juan Cheng, et al. *[full author details at the end of the article]*

Received: 26 March 2018 / Accepted: 12 June 2018 / Published online: 22 June 2018

Abstract

A novel flower-like Bi_2O_4/ZnO heterojunction photocatalyst was synthesized through a facile two-step hydrothermal method and characterized by different technologies. The characterization results indicated that the photoluminescence spectrum of pure ZnO was greatly reduced by the formation of heterojunction at the interface of ZnO and Bi_2O_4 and the photocurrent intensity of the catalyst was 6.4 μA, which was 4.9 times higher than that of pure ZnO, resulting in an efficient separation of electron–hole pairs. The experimental results displayed that the as-prepared heterojunction of (1:3) Bi_2O_4/ZnO effectively prevented the agglomeration of nano-ZnO in aqueous solution and had a great high photocatalytic activity on degrading methylene blue and tetracycline under visible light. The photodegradation rates of (1:3) Bi_2O_4/ZnO for methylene blue and tetracycline were approximately 380 and 309.5 times higher than those of pure ZnO, respectively, and 95.68% of methylene blue and 85.68% of tetracycline were degraded under visible light within half an hour. The mineralization results showed that the two pollutants were firstly decomposed into intermediate products and then further fully mineralized. The results also indicated that the catalyst of (1:3) Bi_2O_4/ZnO had good stabilization and high reusability. Moreover, reactive species of $\cdot O_2^-$ and h^+ were proved to play a dominant role on accelerating the process of degradation. In the end, the detailed mechanism of photocatalytic degradation was proposed.

Electronic supplementary material The online version of this article (https://doi.org/10.1007/s11164-018-3509-7) contains supplementary material, which is available to authorized users.

Graphical Abstract

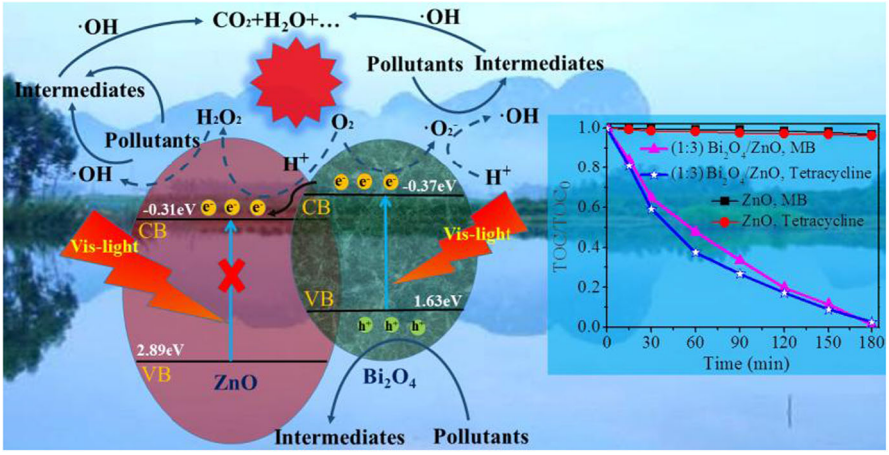

Keywords Photocatalysis · Organic contaminants · Antibiotic · Dibismuth tetroxide · Zinc oxide

Introduction

Photocatalytic technology has attracted much attention owing to its high efficiency, low energy consumption, easy operation and mild reaction conditions in the control of water pollutants [1–4]. At present, most studies use titanium dioxide (TiO_2) as a photocatalyst [5–7]. However, as we know, the production process of TiO_2 is complex and even difficult to be used for bulk sewage treatment due to its high cost.

Nowadays, highly photocatalytic semiconductor photocatalysts of zinc oxide (ZnO) with low price, non-toxicity and good stability has become the new research focus on the degradation of various water pollutants [8]. ZnO is a direct transition semiconductor with a forbidden band width of 3.2 eV. Moreover, ZnO has potential values of valence band (VB) and conduction band (CB) similar to anatase TiO_2, as well as higher electron mobility than anatase TiO_2 [9–11].

Nano-ZnO has huge surface energy, which seriously affects the dispersity of nano-ZnO powder in water and the performance of final product, easily resulted in the occurrence of agglomeration [12–14]. In addition, like TiO_2, ZnO only responds in the UV range, which has great constraints on its practical application [15–17]. Therefore, it is necessary to broaden the range of absorption spectra of ZnO. Common methods mainly form semiconductor composites through simple combination, heterophase combination, doping metal and non-metal ions or form multilayer structure with narrow band gap semiconductor materials [18–20].

The semiconductor composites can overcome the disadvantage of low quantum efficiency, enlarge the specific surface area, increase the active sites, reduce the forbidden band width, improve the kinetic conditions of photocatalytic reaction and charge separation efficiency and extend spectral response range of a single semiconductor catalyst. Some semiconductor composites such as CdS [21], In_2S_3 [22], NiO [23], CuO [24], SnO [25], Zn_2TiO_4 [26], CeO_2 [27], Bi_2O_3 [28], $BiVO_4$ [29], ZrO_2 [30] and Bi_2WO_6 [31] are commonly employed.

Recently, a new visible-light-driven photocatalyst of Bi_2O_4 was synthesized and used to photodegrade organic contaminants [32]. It is a simple oxide with a narrow band gap ($\sim$ 2.0 eV) and a mixed valence of Bi^{3+} and Bi^{5+}, exhibiting better photocatalytic activity than other visible light catalysts such as CdS and Bi_2O_3 [33–35]. However, there is a paucity of literature reporting about the complex semiconductor composites of Bi_2O_4 except Fe_3O_4/Bi_2O_4 [36], Bi_2O_4 @TiO_2 [37] and $Bi_2O_2CO_3/Bi_2O_4$ [38].

As we know, a heterojunction with a space charge region at the interface of different semiconductors is formed owing to the diffusion of electrons and holes when different semiconductors are combined together. The formed heterojunction is very conducive to the photocatalytic activity of semiconductors.

In view of the importance of heterojunction for photocatalysis, some new discoveries about semiconductor heterojunction have been reported, such as Bi@BiOCl [39], BiOCl/BiOBr [40] and Bi_2WO_6/ZnO [41].

In this study, to improve the photocatalytic activity of nano-ZnO and simultaneously prevent its agglomeration, a novel and flower-like heterojunction photocatalyst of Bi_2O_4/ZnO was synthesized through a facile two-step hydrothermal method. Meanwhile, the photocatalytic activity of the as-prepared heterojunction photocatalyst of Bi_2O_4/ZnO was determined through degrading dyes and antibiotics under visible light irradiation. In the end, the mechanism of photocatalytic degradation of heterojunction Bi_2O_4/ZnO was predicted based on experimental and characterization results.

Materials and methods

Chemicals and reagents

Sodium bismuthate hydrate ($NaBiO_3{\cdot}2H_2O$, 85.0%), citric acid (99.5%), zinc acetate dihydrate, sodium hydroxide (NaOH, 96%), sodium oxalate ($Na_2C_2O_4$), Isopropanol (IPA) and 4-hydroxy-2, 2, 6, 6-tetramethylpiperidinyloxy (TEMPOL) were of analytical grade. Both methylene blue (MB, $\geq$ 92%) and tetracycline ($\geq$ 98%) were procured from Macklin Reagents (Shanghai) Co., Ltd.

Synthesis of ZnO sample

A certain amount of zinc acetate (0.02 mol) and citric acid (0.014 mol) were dissolved in a certain volume of ethanol solution (80 mL, 20%, v/v). The mixed solution was stirred vigorously, and then a certain amount of NaOH solution (10 M)

was added to adjust the solution pH to 13 measured via a pH instrument. After that, the solution was transferred into a Teflon-lined autoclave at 423 K for 15 h. After cooling down, the obtained solid substance was washed and filtered and then dried at 373 K. Finally, the products were calcined at 773 K for 2 h to obtain ZnO nanoparticles.

Synthesis of Bi_2O_4/ZnO photocatalysts

A certain amount of 0.632 g $NaBiO_3 \cdot 2H_2O$ was dissolved in bottled deionized water (80 mL) and then treated by sonication for 30 min. After that, as-prepared ZnO nanoparticles were added into the solution with varied molar ratios of Bi_2O_4 and Zn = 1: 1, 1: 3, 1: 5 and 1: 10 and sonicated for 30 min. A suspension containing ZnO nanoparticles was formed.

The suspension was transferred into a Teflon-lined autoclave and retained for 12 h at 413 K. After cooling down, the obtained samples were washed, filtered and then dried at 333 K overnight. The final products were marked as (1:1) Bi_2O_4/ZnO, (1:3) Bi_2O_4/ZnO, (1:5) Bi_2O_4/ZnO and (1:10) Bi_2O_4/ZnO based on the various molar ratios of Bi_2O_4 and ZnO.

Characterization

X-ray diffraction (XRD) profile was determined via an X-ray diffractometer (Bruker D8, Germany). Scanning electron microscopy (SEM, FEI Quanta FEG250, USA) and transmission electron microscopy (TEM, JEM-2100, Japan) were used to detect the morphology of Bi_2O_4/ZnO. The chemical composition was determined by an X-ray photoelectron spectrometer (XPS, Escalab 250Xi, USA). UV–visible diffuse reflectance spectroscopy (UV–DRS, Shimadzu UV-3600, Japan) was measured on a UV–vis spectrophotometer. Photoluminescence (PL) spectroscopy spectra and photocurrent intensity were measured on a Horiba iHR-550 fluorescence spectrophotometer and an electrochemical workstation (CHI 660E, Chenhua Instrument Company), respectively.

Photocatalytic activity

The photocatalytic activity of Bi_2O_4/ZnO catalysts was determined through degrading methylene blue (MB) [42] and tetracycline under vis-light irradiation. Typically, 50.0 mg of Bi_2O_4/ZnO were dissolved in a given amount of MB (100 mL, 10 mg/L) or tetracycline solution (100 mL, 20 mg/L). The mixed solution was stirred vigorously in the dark for 30 min until adsorption equilibrium was obtained. A 500 W xenon lamp equipped with a 420-nm cut-off filter was used to simulate a visible light source.

During the process of photodegradation, a certain amount of mixed solution containing catalysts was taken at certain intervals, filtered and then measured by UV-DRS to determine residual concentration of MB at an adsorption wavelength of 664 nm or tetracycline at 350 nm. Degradation efficiency was calculated based on

the equilibrium concentration (C_0, mg/L) and the residual concentration (C_t, mg/L) after irradiation at any time t (min).

Active species trapping experiments

In order to explore the photocatalytic mechanism of Bi_2O_4/ZnO catalysts and determine what predominant active species was during the process of photocatalysis, trapping experiments with a several active radicals were examined. In general, main active species involved in photocatalysis include superoxide radicals ($\cdot O_2^-$), holes (h^+) and hydroxyl radicals (·OH). In the present experiment, a given amount (1.0 mmol/L) of isopropanol (IPA), $Na_2C_2O_4$ and 4-hydroxy-2, 2, 6, 6-tetramethylpiperidinyloxy (TEMPOL) were employed as scavengers to capture ·OH, h^+ and $\cdot O_2^-$, respectively [43–45].

Results and discussion

Structural and morphology characterizations

XRD

The purity and phase structure of the prepared samples were characterized by XRD, as shown in Fig. 1. It can be seen that the diffraction peaks of ZnO nanoparticles coincided with those of hexagonal wurtzite ZnO (JCPDS No. 36-1451) [46], and the main characteristic peaks of ZnO nanoparticles appeared at 31.8°, 34.4°, 36.3°, 47.7°, 56.7° and 63.0°, corresponding to the crystal planes of (100), (002), (101), (102), (110) and (103), respectively. The main characteristic peaks of Bi_2O_4 appeared at 26.9°, 29.5°, 30.4° and 32.5° and coincided with those of monoclinic

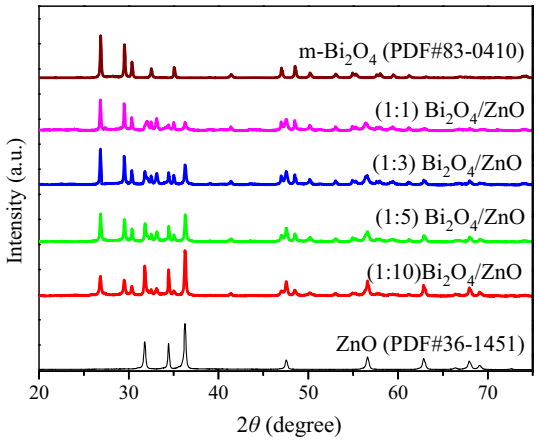

Fig. 1 XRD of the photocatalysts

phase Bi_2O_4 (JCPDS No. 83-0410), assigned to crystal planes of (111), (−311), (400) and (−202) [47].

XRD patterns of four samples showed that no other impurity peaks were observed except the characteristic peaks of ZnO and Bi_2O_4, indicating that composite materials of Bi_2O_4/ZnO were successfully synthesized through incorporating Bi_2O_4 into ZnO by a hydrothermal method.

Compared with pure ZnO and Bi_2O_4, the relative peak height were changed obviously with the increase of Bi_2O_4 content, indicating that Bi_2O_4 may be incorporated into the lattices of ZnO to produce some crystal defects or form a kind of new composites of Bi_2O_4/ZnO heterojunction. In addition, the relative peak intensities among Bi_2O_4/ZnO heterojunctions were closely related to different molar ratios of Bi_2O_4 and ZnO (1:1, 1:3, 1:5 and 1:10).

SEM

Figure 2a, b are SEM figures of the as-prepared ZnO nanoparticles, which clearly showed that the samples completely consisted of a micron-sized nanostructured pompon-like flower with a diameter of 4.6 μm. Figure 2c is the SEM figure of Bi_2O_4 nanoparticles with granular structure. Figure 2d and 2e shows that Bi_2O_4 nanoparticles were attached onto the flower-like structure of ZnO, which was conducive to preventing the agglomeration of nano-ZnO in aqueous solution. Moreover, there were no other impurity peaks observed except the characteristic peaks of ZnO and Bi_2O_4 based on the diffraction peak of XRD as shown in Fig. 1. Figure 2f is the picture of as-prepared catalyst of (1:3) Bi_2O_4/ZnO.

From the TEM image of the sample shown in Fig. 3a, it can be seen that the pompons are inlaid by many small particles. In addition, the HRTEM (Fig. 3b) and XRD images also further confirmed that Bi_2O_4 particles were successfully attached onto the flower-like structure of ZnO.

HRTEM

The lattice spacing measured from the HRTEM figure was 0.26 nm, conforming to the (002) plane of hexagonal wurtzite ZnO, and the lattice spacing of 0.332 and 0.294 nm corresponded to the (111) and (400) planes of monoclinic phase Bi_2O_4, respectively. It can be seen from the HRTEM figure that the two n-type semiconductor materials are in close contact, due to the diffusion of electrons and holes, an n–n junction will be formed at the interface with the space charge region [48–50]. In addition, the porous structure property indicated that Brunauer–Emmett–Teller (BET) values of ZnO and (1:3) Bi_2O_4/ZnO were 3.81 and 9.69 m^2/g (Fig. S1), respectively. These structural and morphology characterizations were all conducive to enhancing the photocatalytic performance of catalysts.

Analysis of chemical state

Figure 4a is the XPS survey spectra of (1:3) Bi_2O_4/ZnO, which mainly consisted of Bi, O, Zn and C elements, indicating that there was no impurity introduced into the

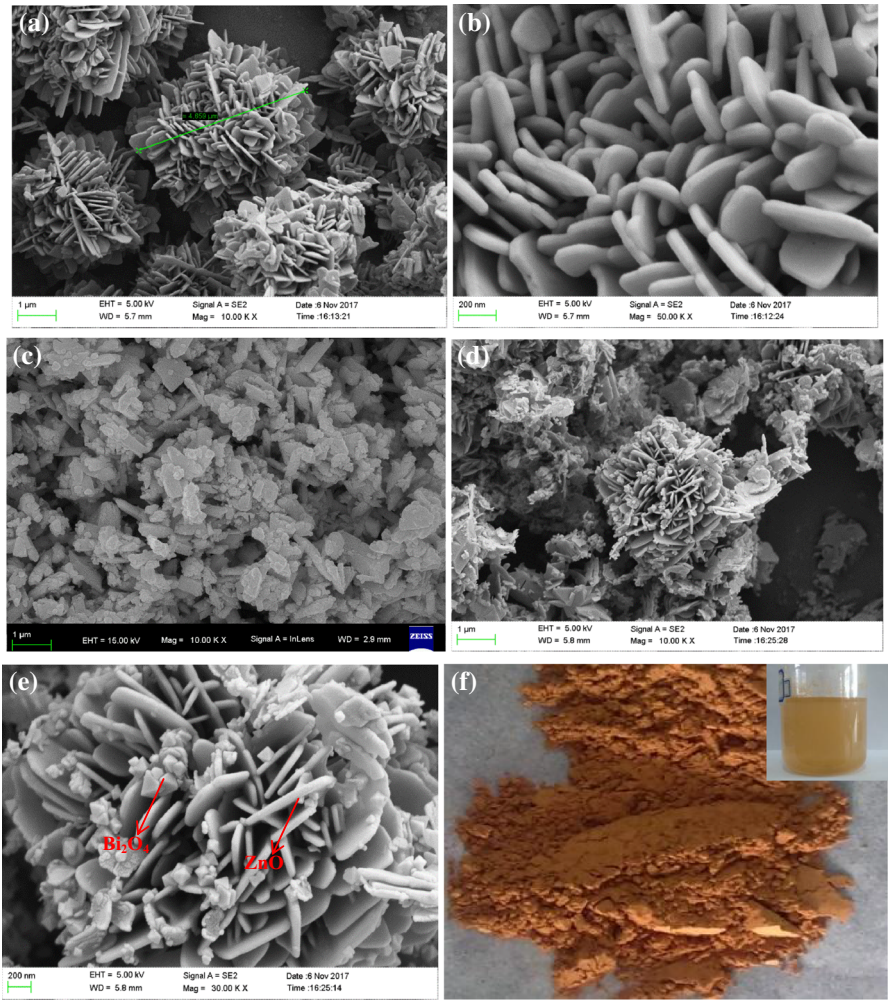

Fig. 2 SEM of ZnO (**a**) and (**b**), Bi_2O_4 (**c**), (1:3) Bi_2O_4/ZnO (**d**) and (**e**) and picture of (1:3) Bi_2O_4/ZnO (**f**)

composite material. Figure 4b spectra shows that the Bi $4f_{5/2}$ (or Bi $4f_{7/2}$) peak in (1:3) Bi_2O_4/ZnO heterostructure can be resolved well into two bimodal peaks at binding energies of 163.6 and 164.4 eV (or at 158.2 and 159.1 eV). According to previous literature, the two observed peaks are attributed to Bi^{3+} and Bi^{5+}, respectively [51].

As shown in Fig. 4c, the asymmetric O1*s* peak can be decomposed into three peaks at 530.3, 531.2 and 533.2 eV. It is indicated that there were three types of oxygen in (1:3) Bi_2O_4/ZnO heterostructure. The binding energy at 530.1 eV can be indexed to lattice oxygen in Zn–O bonds [52]. The two peaks located at 529.9 and 531.0 eV correspond to $O-Bi^{3+}$ and $O-Bi^{5+}$ bonds in Bi_2O_4, respectively [51].

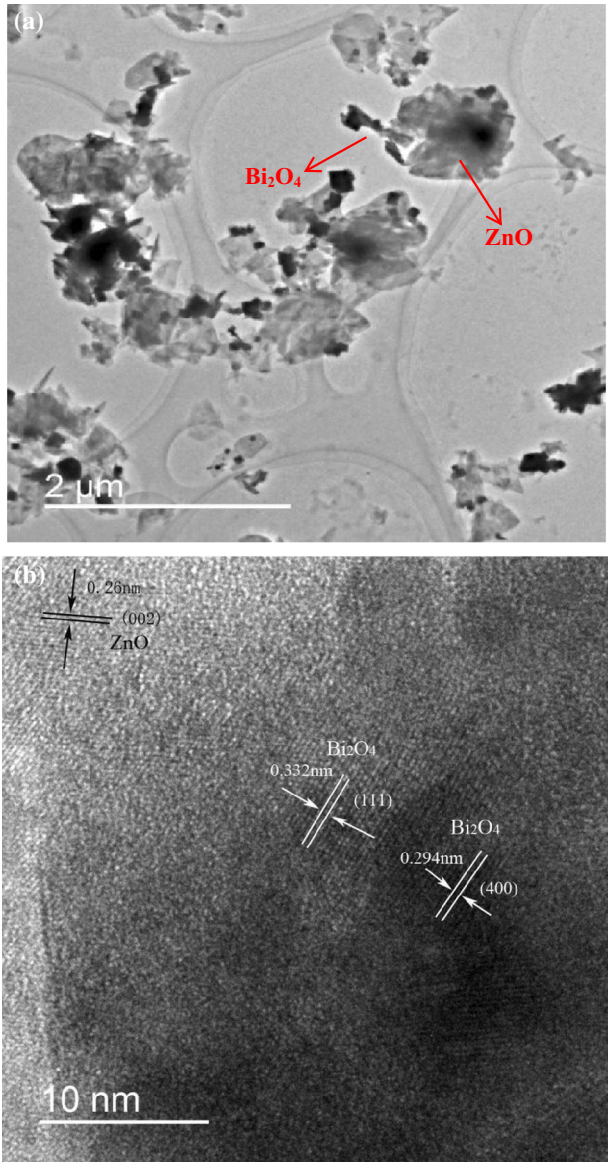

Fig. 3 TEM (**a**) and HR-TEM (**b**) images of (1:3) Bi_2O_4/ZnO heterojunction

In Fig. 4d, the binding energies exhibited by Zn 2*p* were located at 1021.6 and 1044.7 eV, respectively, corresponding to Zn $2p_{3/2}$ and Zn $2p_{1/2}$ [52]. This shows that Zn element was in the form of Zn^{2+} in Bi_2O_4/ZnO heterostructure. The peak located at 284.6 eV was indexed to C 1 *s* (Fig. S2), which was caused by foreign carbon on the surface of the equipment, but it had nothing to do with the sample.

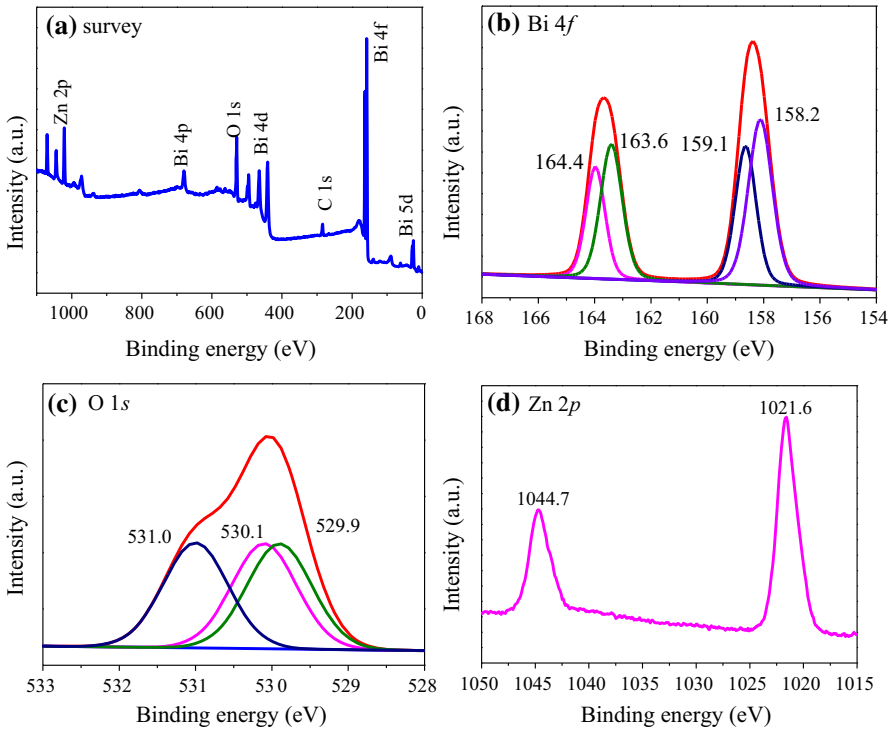

Fig. 4 XPS patterns of survey scan (**a**), Bi 4*f* (b), O 1*s* (**c**) and Zn 2*p* (**d**) of (1:3) Bi_2O_4/ZnO

DRS property

Photocatalytic efficiency of catalysts is closely related to the absorption properties for light [53]. The test method used the integration sphere method to collect all the diffuse light. As shown in Fig. 5a, the pure Bi_2O_4 sample showed a wide range of light absorption with an edge located at 610 nm in the visible light region. The as-prepared ZnO nanoparticles only had a fundamental absorption band in the ultraviolet region. However, the absorption bands of four types of catalysts of Bi_2O_4/ZnO shifted to the visible region due to the narrow band gap of Bi_2O_4. The absorption wavelength of Bi_2O_4/ZnO composites was extended to the visible region and red-shifted from original 650 nm of Bi_2O_4 to 800 nm.

By comparison, the absorption of catalysts of Bi_2O_4/ZnO in the visible region increased remarkably due to the addition of Bi_2O_4 with visible light response. The band gap energy of the catalysts can be calculated using the following formula:

$$\alpha = A\left(hv - E_g\right)^{n/2}/hv \tag{1}$$

where, α, A and h are absorption coefficient, a constant and Planck's constant, respectively. E_g, v and n are the direct transitions with energy, incident light frequency and a value of 1, respectively [54]. The corresponding reflected spectra of

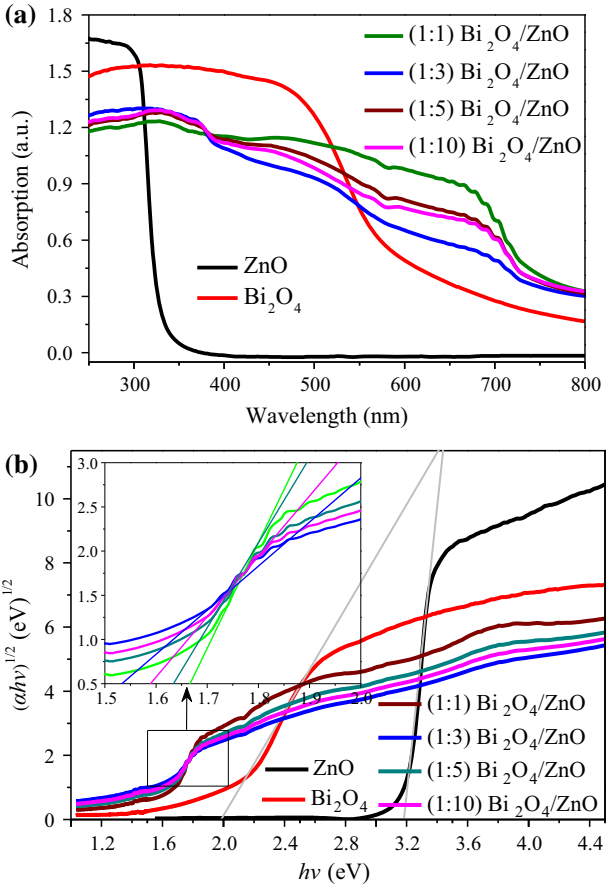

Fig. 5 UV–visible spectra of ZnO and Bi_2O_4/ZnO (**a**) and band gap values (**b**)

the Kubeka-Munch transform showed that the value of the point of intersection of the tangent to the interpolated curve and the horizontal axis in Fig. 5b were the values of band gap energy. The obtained band gap energies of ZnO particles, Bi_2O_4 particles, (1:1) Bi_2O_4/ZnO, (1:3) Bi_2O_4/ZnO, (1:5) Bi_2O_4/ZnO and (1:10) Bi_2O_4/ZnO were 3.2, 2.0, 1.67, 1.54, 1.64 and 1.59 eV, respectively.

Evaluation of photocatalytic activity

The colored organic dyes in water bodies released from the textile and dye industries are hardly biodegradable and can severely damage aquatic ecosystems and aquatic organisms. The photocatalytic degradation of organic pollutants under visible light or ultraviolet light is an important method to eliminate pollution, as it can quickly and thoroughly eliminate pollutants without leaving any harmful residue. Rajabi et al. achieved a series of remarkable results using methylene blue doped with metal ions to remove dye [55–57].

Tetracycline, a type of antibiotic substance used in planting and breeding areas, widely exists in surface water, groundwater and soil because it has limited biodegradation and is not efficiently degraded by traditional water treatment technology [58–60].

Hence, the activity of the as-prepared catalysts was evaluated by degrading MB, as well as tetracycline. To verify that the degradation of MB and tetracycline was not caused by photolysis, the experiments were firstly carried out without catalysts under the irradiation of visible light. As shown in Fig. 6a, c, there was no obvious degradation observed under the conditions of irradiation and without catalysts, indicating the stability of MB and tetracycline under the irradiation of visible light.

After the catalysts were added into the solution, the concentration of MB and tetracycline in solution decreased gradually with the increasing time, as shown in Fig. 6a, c. Moreover, the position of maximum adsorption peak of the two organic pollutants had scarcely any shift while the peak intensity decreased gradually with the increasing time and finally disappeared after 30 min irradiation, as shown in Fig. 6b, d [61].

Figure 6 also showed that the optimum catalyst of (1:3) Bi_2O_4/ZnO) had the highest degradation efficiency of 98.5% for MB and 90.5% for tetracycline within 30 min compared with the other four catalysts.

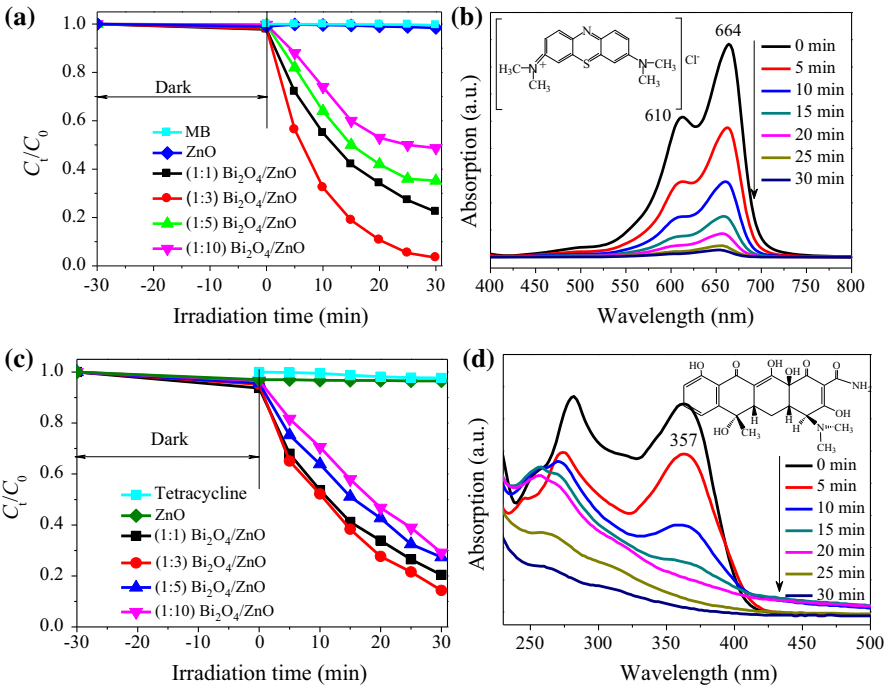

Fig. 6 Degradation and spectral changes of 10 mg/L MB (**a**), (**b**) and 20 mg/L tetracycline (**c**), (**d**). Conditions: pH = 7, dosage of 0.5 g/L and T = 298 K

Kinetics

The kinetic model of Langmuir–Hinshelwood [62] was employed to further describe the degradation behaviour of MB and tetracycline through fitting the degradation data. The plots of $-ln(C_t/C_0)$ versus irradiation time of t are shown in Fig. 7. Based on the data, all degradation data were well fitted by the Langmuir–Hinshelwood model and have very high correlation coefficient ($R^2 > 0.92$) as listed in Table 1.

Based on the fitting results shown in Fig. 7, the pure ZnO catalyst had little photocatalytic ability for MB or tetracycline. However, the photodegradation efficiency of the as-prepared catalyst of (1:3) Bi_2O_4/ZnO for MB was approximately 241 times higher than that of pure ZnO, and for tetracycline, the figure was 244.8 times.

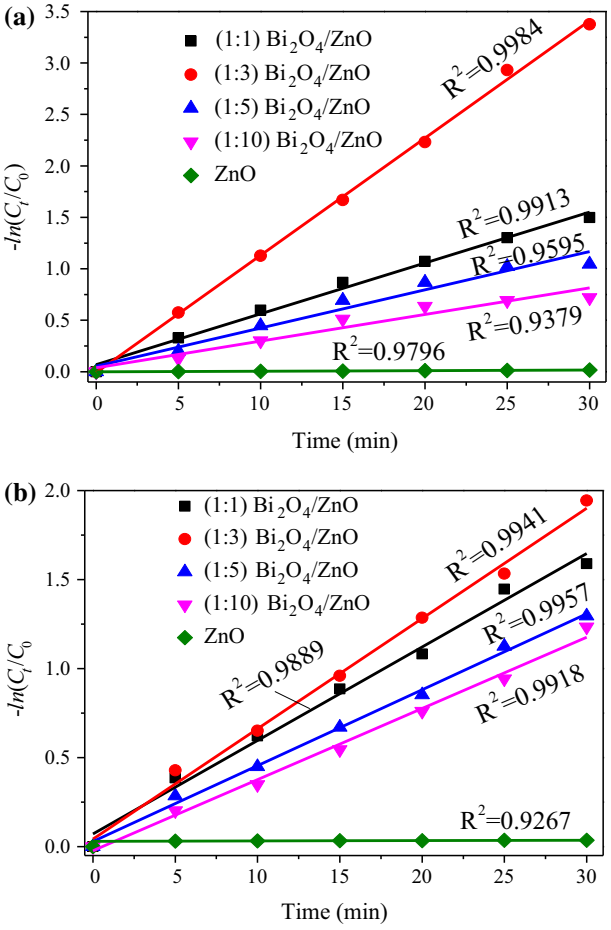

Fig. 7 Linear plots of $-\ ln(C_t/C_0)$ versus time for MB (**a**) and tetracycline (**b**)

Table 1 Photocatalytic results of MB (10 mg/L) and tetracycline (20 mg/L)

Catalysts	Photocatalytic efficiency (%)		Rate constant k (min^{-1})		R^2	
	MB	Tetracycline	MB	Tetracycline	MB	Tetracycline
(1:1) Bi_2O_4/ZnO	77.65	79.59	0.0494	0.0525	0.9913	0.9889
(1:3) Bi_2O_4/ZnO	96.58	85.68	0.1139	0.0619	0.9984	0.9941
(1:5) Bi_2O_4/ZnO	64.8	72.63	0.0371	0.0427	0.9595	0.9957
(1:10) Bi_2O_4/ZnO	51.29	70.89	0.0258	0.0302	0.9379	0.9918
ZnO	0.40	0.35	0.0003	0.0002	0.9796	0.9267

Meanwhile, the photodegradation rate of the catalyst of (1:3) Bi_2O_4/ZnO for MB was about 380 times higher than that of pure ZnO, and for tetracycline, the figure reached 309.5. The results indicated that the incorporation of Bi_2O_4 into ZnO was great beneficial for the promotion of photocatalytic performance of ZnO, which can be attributed to effective separation of electron–hole in the composite Bi_2O_4/ZnO. The corresponding values for different catalysts were listed in Table 1.

The degradation effect of (1:3) Bi_2O_4/ZnO in the present study surpassed the photocatalytic performance for MB and tetracycline by many other existing catalysts reported recently, as listed in Table S1.

In order to investigate the effect of the photocatalyst dosage on the photocatalytic effect, MB was selected as the target contaminant for the experiment [63–65]. The initial concentration and volume of MB solutions were 10 mg/L and 100 mL, respectively. The dosages of (1:3) Bi_2O_4/ZnO were selected as 0.03, 0.05, 0.07 and 0.1 g. After a dark reaction, a certain volume of supernatant was taken every half an hour to analyse the residual concentration of MB, and the results obtained are

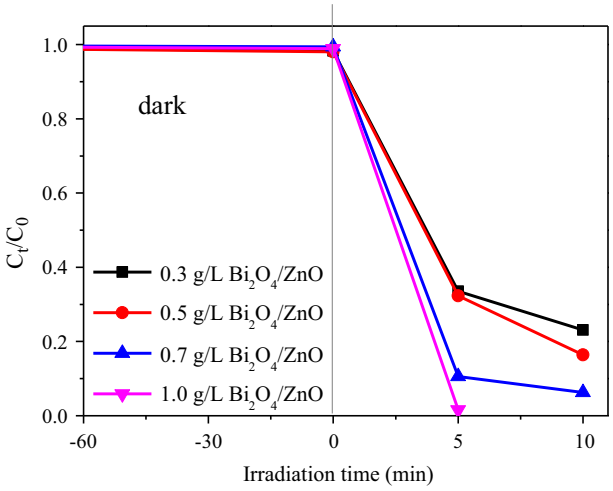

Fig. 8 Different dosages of (1:3) Bi_2O_4/ZnO degradation MB. Conditions: pH = 7, C_0 = 10 mg/L and T = 298 K

shown in Fig. 8. It can be seen from the figure that the photocatalytic efficiency gradually increased with the increase of (1:3) Bi_2O_4/ZnO dosage, indicating that the dosage of photocatalyst was favourable to the light utilization and the photocatalytic efficiency.

Mineralization

In fact, good photodegradation effect for organic compounds does not definitely mean complete mineralization because some intermediate products may be produced [36]. Therefore, in order to further and deeply confirm the effect of as-prepared catalysts on MB and tetracycline, the values of total organic carbon (TOC) were determined at any irradiation time, and the results are shown in Fig. 9.

From Fig. 9, it can be seen that the removal efficiencies of TOC with catalyst (1:3) Bi_2O_4/ZnO for MB and tetracycline 35.2 and 42.8%, respectively. Meanwhile, the efficiencies of pure ZnO were nearly zero. The results indicated that there was about 70% TOC of MB or 60% TOC of tetracycline in the solution, namely, a great deal of intermediate products had being formed accompanying by the process of photocatalysis, although a great high photodegradation effect was achieved.

The experimental results also showed that the two pollutants were completely mineralized into H_2O and CO_2 with the prolonging of time to 3 h. Obviously, the as-prepared composite (1:3) Bi_2O_4/ZnO had the advantages of quick and complete degradation for MB and tetracycline and was a potential and promising photocatalyst, compared with pure ZnO.

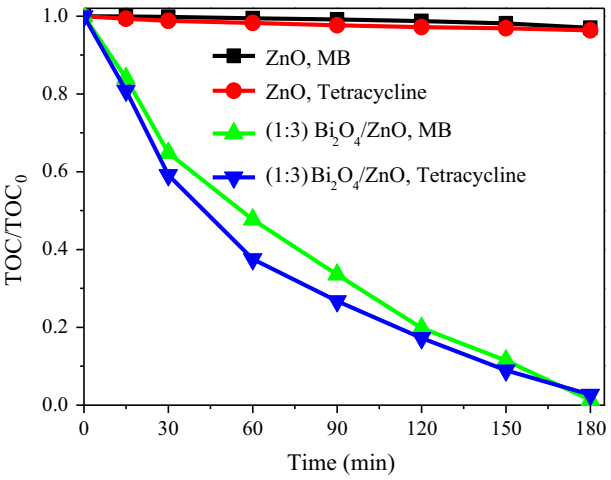

Fig. 9 Mineralization of MB (10 mg/L) and tetracycline (20 mg/L) over ZnO and (1:3) Bi_2O_4/ZnO (0.5 g/L) under visible light irradiation

Reusability

The reusability of photocatalysts is of quite importance for their application in the environmental remediation. For this consideration, the XRD patterns of (1:3) Bi_2O_4/ZnO before and after the photocatalytic reaction [66] and the recycling experiments of catalysts were carried out to evaluate their reusability after five recycling photocatalytic reactions for the degradation of MB and tetracycline at the same conditions as before [67]. When each recycling experiment finished, the catalysts were filtered and washed with deionized water for 30 min.

There was clearly no remarkable change in peak shape and addition peaks appeared, demonstrating that the excellent crystal structure of (1:3) Bi_2O_4/ZnO as shown in Fig. 10a.

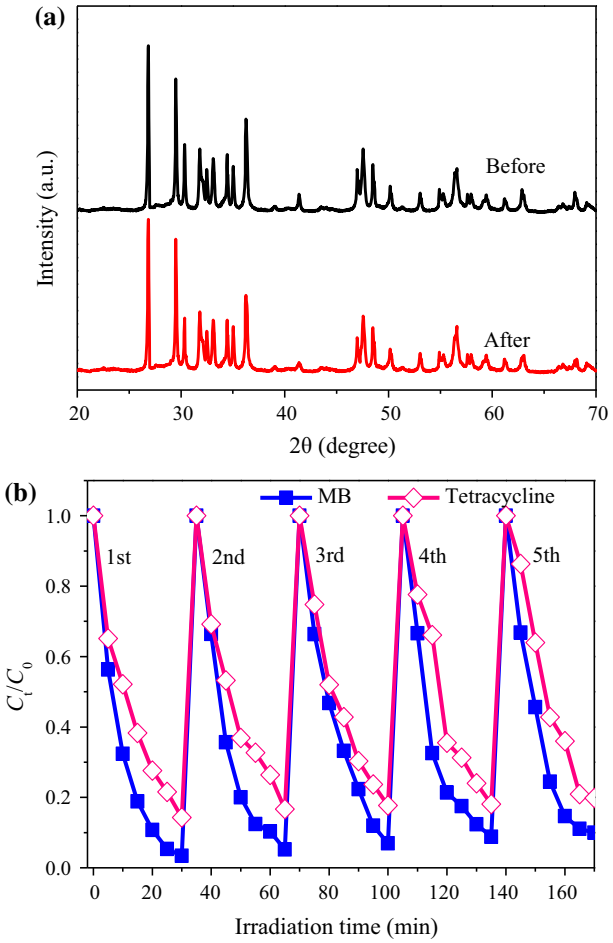

Fig. 10 XRD patterns of (1:3) Bi_2O_4/ZnO before and after photocatalytic reaction (**a**); Recycling experiments for degradation of MB (10 mg/L) and tetracycline (20 mg/L) over (1:3) Bi_2O_4/ZnO (0.5 g/L) (**b**)

From Fig. 10b, it can be seen that no remarkable decline of photocatalytic capability was observed after five recycling experiments, exhibiting good stabilization and high reusability. Despite the high reusability, the real application parameters and efficiencies should be considered carefully and deeply in further research.

Photoluminescence and photocurrents

The PL spectrum is an effective and convenient technology to evaluate recombination efficiency of charge carriers. In general, PL intensity is proportional to recombination rate of photo-generated carriers, and high intensity implies low photocatalytic efficiency [68, 69].

PL spectra of pure ZnO and Bi_2O_4 were presented in Fig. 11. For the composite materials, the intensity of the emission band was significantly reduced. This results show that the Bi_2O_4 can improve the separation of photoelectron–hole pairs through being incorporated into ZnO.

The electrical properties of the obtained catalysts were investigated by testing their photocurrent intensities under visible light. Under lighting, the current quickly appeared and reached a relatively stable stage after 200 s, as shown in Fig. 12. The photocurrent produced by the composites of Bi_2O_4/ZnO was about 6.4 μA under visible light irradiation, which was 4.9 times higher than that of pure ZnO.

The results show that the separation efficiency of photocatalytic electron–hole pairs of the composite Bi_2O_4/ZnO was obviously enhanced, which was in coincident with the excellent photocatalytic performance of the composite Bi_2O_4/ZnO as presented above.

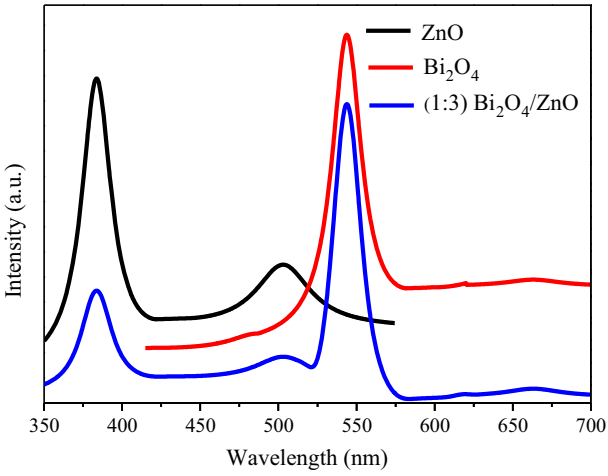

Fig. 11 PL spectra of photocatalysts

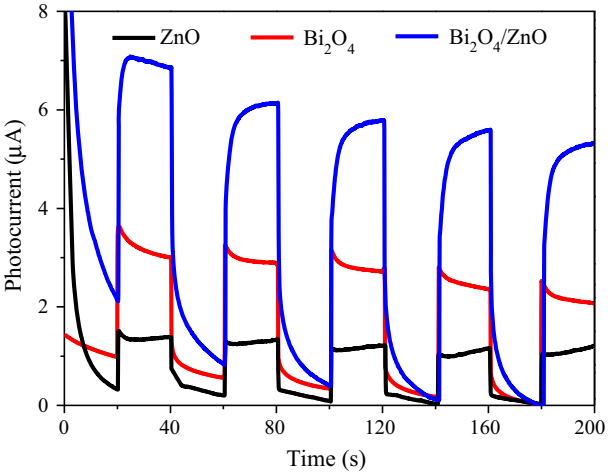

Fig. 12 Transient photocurrent response of ZnO, Bi_2O_4 and (1:3) Bi_2O_4/ZnO samples

Photocatalytic mechanism

From the trapping experiment results shown in Fig. 13a, three types of scavengers including TEMPOL, IPA and $Na_2C_2O_4$ had a different degree of inhibition against the photodegradation of MB. When IPA (·OH quencher) was added, the effect of as-prepared composites on photodegradation of MB was not obvious, which meant that ·OH was not the main active factor.

Photocatalytic degradation of MB was significantly inhibited due to the addition of TEMPOL ($\cdot O_2^-$ quencher) and $Na_2C_2O_4$ (h^+ quencher), resulting in a little photodegradation of MB, indicating that $\cdot O_2^-$ radicals and h^+ played a dominant role during the process of photocatalytic degradation, compared to ·OH radicals. The corresponding values of rate constant k also indicated these results, which were 113.90, 56.28, 0.11 and 2.41 min^{-1} presented in Fig. 13b.

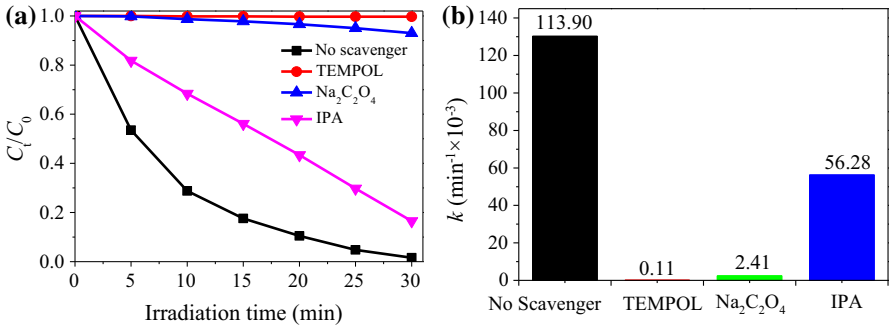

Fig. 13 Photodegradation of MB (10 mg/L) over (1:3) Bi_2O_4/ZnO (0.5 g/L) heterojunction with different scavengers: No scavenger, TEMPOL, IPA and $Na_2C_2O_4$. Conditions: pH = 7, dosage of Bi_2O_4/ZnO = 0.5 g/L, dosage of scavengers = 1 mmol/L and T = 298 K

From Fig. 13, it can be concluded that the order of active radicals were $\cdot O_2^-$ (major), h^+ (major) and ·OH (minor or negligible) radicals based on their roles in the photocatalytic degradation of MB.

The relative band positions of Bi_2O_4 and ZnO were calculated according to following Eq. (2) to further explore the mechanism of Bi_2O_4/ZnO heterojunction.

$$E_{CB} = X - 0.5E_g + E_0 \quad (2)$$

where E_{CB}, E_g, E_0, and X are the conduction band (CB) value, band gap energy of catalysts, energy of free electrons on hydrogen and electronegativity of semiconductors (here, 5.79 eV), respectively [70]. The band gap energies of ZnO and Bi_2O_4 were 3.2 and 2.0 eV, respectively. The values of E_{CB} and valence band (VB) of ZnO and Bi_2O_4 were − 0.31 and − 0.37 eV, 2.89 and 1.63 eV on the basis of Eq. (2), respectively.

Based on the experimental results and energy band theory, the possible mechanism of photo-degradation of organic compounds with Bi_2O_4/ZnO heterojunction is predicted in Scheme 1.

Bi_2O_4 has relatively narrow band gap energy of about 2.0 eV and can be excited under visible light. Electron–hole pairs are generated on the VB of Bi_2O_4 by visible light excitation, and these photogenerated electrons are transferred onto the CB of Bi_2O_4, leaving light-induced holes on the VB of Bi_2O_4. Then, the holes directly oxidize organic matter. Meanwhile, as the CB potential of Bi_2O_4 is more negative than that of $O_2/\cdot O_2^-$ (− 0.33 eV) [71], the electrons on the CB of Bi_2O_4 react with adsorbed oxygen $[O_2]_{(ad.)}$ to produce $\cdot O_2^-$, which further combines with H^+ to generate hydroxyl radicals or directly oxidize organic contaminants.

It is clear that both of the values of E_{CB} and E_{VB} of ZnO were higher than those of Bi_2O_4. In addition, the CB band potential of Bi_2O_4 (− 0.37 V vs. NHE) was more negative than that of ZnO (− 0.31 V vs. NHE), so these photoexcited electrons on the CB of Bi_2O_4 can easily transfer onto the CB of ZnO through the formed heterojunction between ZnO and Bi_2O_4.

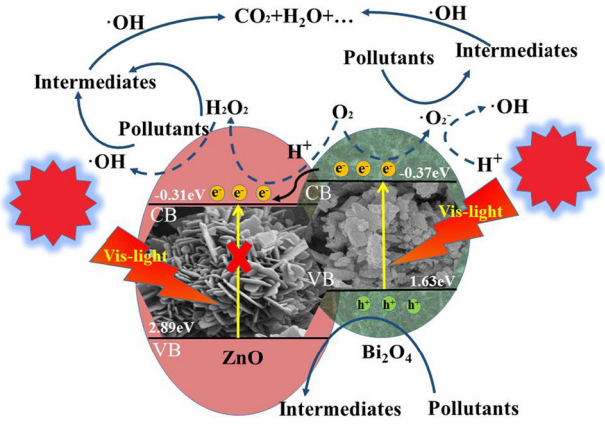

Scheme 1 Schematic illustration of photodegradation process over Bi_2O_4/ZnO

In addition, the CB potential of ZnO is more positive than that of $O_2/^{\cdot}O_2^-$ (− 0.33 eV), but more negative than that of the reaction: $e_{CB}^- + O_2 + H^+ \rightarrow H_2O_2$ (+ 0.682 V vs. NHE) [72]. Therefore, these electrons transferring onto the CB of ZnO react with adsorbed oxygen $[O_2]_{(ad.)}$ and H^+ to form H_2O_2, which may be further reduced to $^{\cdot}OH$ radicals. The generated H_2O_2 and ·OH radicals can degrade organic pollutants through oxidation.

Based on the experimental results, the analysis of energy band theory and the decreased band gap energy of (1:3) Bi_2O_4/ZnO from 3.2 eV (ZnO) to 1.54 eV ((1:3) Bi_2O_4/ZnO), the modification of ZnO with Bi_2O_4 benefited the separation of photogenerated charge carriers and the photocatalytic activity of the Bi_2O_4/ZnO photocatalysts. This photodegradation process can be described in the following equations:

$$Bi_2O_4 \xrightarrow{h\nu} [e^-]_{Bi_2O_4} + [h^+]_{Bi_2O_4} \tag{3}$$

$$\text{Pollutants} \xrightarrow{[h^+]_{Bi_2O_4}} \text{Degraded products} \tag{4}$$

$$[O_2]_{(ad.)} + [e^-]_{Bi_2O_4} \rightarrow \cdot O_2^- \tag{5}$$

$$\cdot O_2^- + 2H^+ \rightarrow 2 \cdot OH \tag{6}$$

$$\cdot O_2^- + \text{Pollutants} \rightarrow \text{Degraded products} \tag{7}$$

$$[e^-]_{Bi_2O_4} + ZnO \rightarrow [e^-]_{ZnO} \tag{8}$$

$$[e^-]_{ZnO} + [O_2]_{(ad.)} + 2H^+ \rightarrow H_2O_2 \tag{9}$$

$$H_2O_2 + [e^-]_{ZnO} \rightarrow \cdot OH + OH^- \tag{10}$$

$$\text{Pollutants} + H_2O_2 \rightarrow \text{Degraded products} \tag{11}$$

$$\text{Pollutants} + \cdot OH \rightarrow \text{Degraded products} \tag{12}$$

where $[e^-]_{Bi_2O_4}$ and $[h^+]_{Bi_2O_4}$ stand for the electrons and holes on Bi_2O_4, respectively.

Conclusions

In summary, based on the characterization and experimental results, a highly efficient heterojunction photocatalyst of Bi_2O_4/ZnO has been successfully synthesized by facile hydrothermal method. Because of the formation of a heterojunction at the interface between ZnO and Bi_2O_4, the separation efficiency of photogenerated electron–hole pairs was greatly increased. The as-synthesized heterojunction photocatalyst of Bi_2O_4/ZnO showed efficient degradation and high reusability for dyes and antibiotics under visible light. The mineralization results showed that less

50% of TOC of two pollutants were degraded within 30 min; however, the two organic pollutants were completely mineralized into H_2O and CO_2 after about 3 h.

The results of free radical scavengers indicated that $^{\cdot}O_2^-$ and H^+ played a dominant role in the decomposition of organic pollutants. Finally, the photocatalytic degradation mechanism of the heterojunction photocatalyst of Bi_2O_4/ZnO was proposed. This study shows that Bi_2O_4/ZnO composite is a novel and efficient photocatalyst for the remediation of polluted water.

Acknowledgement This work was supported by the National Natural Science Foundation of China (No. 51578354) and Six Talent Peaks Program (2016-JNHB-067), Natural Science Research Project of Jiangsu Province Higher Education (2018) and Qing Lan Project of Jiangsu Province.

References

1. C. Yu, W. Zhou, H. Liu, Y. Liu, D.D. Dionysiou, Chem. Eng. J. **287**, 117 (2016)
2. H. Zhang, G. Liu, L. Shi, H. Liu, T. Wang, J. Ye, Nano Energy **22**, 149 (2016)
3. K.R. Reddy, K.V. Karthik, S.B.B. Prasad, S.K. Soni, H.M. Jeong, A.V. Raghu, Polyhedron **120**, 169 (2016)
4. K. Saravanakumar, V. Muthuraj, S. Vadivelb, RSC Adv. **6**, 61357 (2016)
5. X.C. Zhang, W.Y. Hu, K.F. Zhang, J.N. Wang, B.J. Sun, H.Z. Li, P.Z. Qiao, L. Wang, W. Zhou, A.C.S. Sustain, Chem. Eng. **5**, 6894 (2017)
6. J.A. Díaz-Real, G.C. Dubed-Bandomo, J. Galindo-de-la-Rosa, E. Ortiz-Ortega, J. Ledesma-García, L.G. Arriaga, Appl. Catal. B: Environ. **222**, 18 (2018)
7. J. Yan, H. Wu, H. Chen, Y. Zhang, F. Zhang, S.F. Liu, Appl. Catal. B: Environ. **191**, 130 (2016)
8. S.W. Zhao, M. Zheng, X.H. Zou, Y. Guo, Q.J. Pan, A.C.S. Sustain, Chem. Eng. **5**, 6585 (2017)
9. L. Wang, S. Liu, Z. Wang, Y. Zhou, Y. Qin, Z.L. Wang, ACS Nano **10**, 2636 (2016)
10. C.A. Aggelopoulos, M. Dimitropoulos, A. Govatsi, L. Sygellou, C.D. Tsakiroglou, S.N. Yannopoulos, Appl. Catal. B: Environ. **205**, 292 (2017)
11. M. Kwiatkowski, R. Chassagnon, O. Heintz, N. Geoffroy, M. Skompska, I. Bezverkhyy, Appl. Catal. B: Environ. **204**, 200 (2017)
12. X. Shen, D. Mu, S. Chen, B. Wu, F. Wu, A.C.S. Appl, Mater. Interfaces **5**, 3118 (2013)
13. A. Di Mauro, M. Cantarella, G. Nicotra, V. Privitera, G. Impellizzeri, Appl. Catal. B: Environ. **196**, 68 (2016)
14. J. Wang, Y. Xia, Y. Dong, R. Chen, L. Xiang, S. Komarneni, Appl. Catal. B: Environ. **192**, 8 (2016)
15. W. Feng, L. Lin, H. Li, B. Chi, J. Pu, J. Li, Int. J. Hydrogen Energy **42**, 3938 (2017)
16. S. Rehman, R. Ullah, A.M. Butt, N.D. Gohar, J. Hazard. Mater. **170**, 560 (2009)
17. P. Prasannalakshmi, N. Shanmugam, Mater. Sci. Semicond. Proc. **61**, 114 (2017)
18. M.M. Momeni, Y. Ghayeb, J. Mol. Catal. A: Chem. **417**, 107 (2016)
19. F. Wang, L. Liang, L. Shi, M. Liu, J. Sun, ChemPlusChem **80**, 1427 (2015)
20. L. Zhou, L. Wang, J. Zhang, J. Lei, Y. Liu, Res. Chem. Intermed. **43**, 2081 (2016)
21. M. Ding, N. Yao, C. Wang, J. Huang, M. Shao, S. Zhang, P. Li, X. Deng, X. Xu, Nanoscale Res. Lett. **11**, 205 (2016)
22. S. Khanchandani, S. Kundu, A. Patra, A.K. Ganguli, J. Phys. Chem. C **117**, 5558 (2013)
23. P. Dai, T.T. Yan, X.X. Yu, Z.M. Bai, M.Z. Wu, Nanoscale Res. Lett. **11**, 226 (2016)
24. M. Mansournia, L. Ghaderi, J. Alloys Compd. **691**, 171 (2017)
25. C. Lan, J. Gong, Y. Jiang, J. Alloys Compd. **575**, 24 (2013)
26. H.-S. Lim, J. Lee, S. Lee, Y.S. Kang, Y.-K. Sun, K.-D. Suh, Acta Mater. **122**, 287 (2017)
27. Z. Xiong, Z. Lei, Z. Xu, X. Chen, B. Gong, Y. Zhao, H. Zhao, J. Zhang, C. Zheng, J. CO2 Util. **18**, 53 (2017)
28. T.V.L. Thejaswini, D. Prabhakaran, M.A. Maheswari, J. Photochem. Photobiol. A: Chem. **335**, 217 (2017)
29. F. Peng, Y. Ni, Q. Zhou, J. Kou, C. Lu, Z. Xu, J. Alloys Compd. **690**, 953 (2017)
30. C. Fan, S. Yu, G. Qian, Z. Wang, RSC Adv. **7**, 18785 (2017)
31. X. Liu, Q. Lu, J. Liu, J. Alloys Compd. **662**, 598 (2016)

32. D. Wu, L. Ye, S. Yue, B. Wang, W. Wang, H.Y. Yip, P.K. Wong, J. Phys. Chem. C **120**, 7715 (2016)
33. A. Hameed, M. Aslam, I.M.I. Ismail, N. Salah, P. Fornasiero, Appl. Catal. B: Environ. **163**, 444 (2015)
34. D. Xia, W. Wang, R. Yin, Z. Jiang, T. An, G. Li, H. Zhao, P.K. Wong, Appl. Catal. B: Environ. **214**, 23 (2017)
35. M. Maryam, H. Akram, N. Nasrin, R. Mohadeseh, S. Hossein, Iran. Chem. Commun. **3**, 283 (2015)
36. D. Xia, I.M.C. Lo, Water Res. **100**, 393 (2016)
37. X. Li, C. Zhang, C. Hu, L. Xu, Q. Hu, S. Duo, W. Li, Y. Kang, J. Clust. Sci. **28**, 2409 (2017)
38. J. Wang, K. Chen, Y. Shen, X. Wang, Y. Guo, X. Zhou, R. Bai, Res. Chem. Intermed. **44**, 3061 (2018)
39. F. Dong, T. Xiong, S. Yan, H. Wang, Y. Sun, Y. Zhang, H. Huang, Z. Wu, J. Catal. **344**, 401 (2016)
40. L. Ye, L. Wang, H. Xie, Y. Su, X. Jin, C. Zhang, Energy Technol. **3**, 1115 (2015)
41. J. Cheng, Y. Shen, K. Chen, X. Wang, Y. Guo, X. Zhou, R. Bai, Chin. J. Catal. **39**, 810 (2018)
42. K. Saravanakumar, V. Muthuraj, M. Jeyaraj, Spectrochim. Acta Mol. Biomol. Spectrosc. **188**, 291 (2018)
43. Y. Ding, F. Yang, L. Zhu, N. Wang, H. Tang, Appl. Catal. B: Environ. **164**, 151 (2015)
44. C.-Y. Wang, X. Zhang, H.-B. Qiu, W.-K. Wang, G.-X. Huang, J. Jiang, H.-Q. Yu, Appl. Catal. B: Environ. **200**, 659 (2017)
45. N. Tian, Y. Zhang, H. Huang, Y. He, Y. Guo, J. Phys. Chem. C **118**, 15640 (2014)
46. A. Ashar, M. Iqbal, I.A. Bhatti, M.Z. Ahmad, K. Qureshi, J. Nisar, I.H. Bukhari, J. Alloys Compd. **678**, 126 (2016)
47. D. Xia, W. Wang, R. Yin, Z. Jiang, T. An, G. Li, H. Zhao, P.K. Wong, Appl. Catal. B: Environ. **214**, 23 (2017)
48. W. Zhao, Y. Liu, Z. Wei, S. Yang, H. He, C. Sun, Appl. Catal. B: Environ. **185**, 242 (2016)
49. Y. Hu, D. Li, F. Sun, Y. Weng, S. You, Y. Shao, J. Hazard. Mater. **301**, 362 (2016)
50. H. Huang, K. Xiao, Y. He, T. Zhang, F. Dong, X. Du, Y. Zhang, Appl. Catal. B: Environ. **199**, 75 (2016)
51. M. Sun, S. Li, T. Yan, P. Ji, X. Zhao, K. Yuan, D. Wei, B. Du, J. Hazard. Mater. **333**, 169 (2017)
52. Y. Guo, S. Lin, X. Li, Y. Liu, Appl. Sur. Sci. **384**, 83 (2016)
53. A. Rauf, M.S.A. Sher Shah, G.H. Choi, U.B. Humayoun, D.H. Yoon, J.W. Bae, J. Park, W.-J. Kim, P.J. Yoo, ACS Sustain. Chem. Eng. **3**, 2847 (2015)
54. Y. Huang, W. Fan, B. Long, H. Li, F. Zhao, Z. Liu, Y. Tong, H. Ji, Appl. Catal. B: Environ. **185**, 68 (2016)
55. H.R. Rajabi, O. Khani, M. Shamsipur, V. Vatanpour, J. Hazard. Mater. **250–251**, 370 (2013)
56. H.R. Rajabi, M. Farsi, J. Mol. Catal. A: Chem. **399**, 53 (2015)
57. H.R. Rajabi, M. Farsi, Mater. Sci. Semicond. Proc. **48**, 14 (2016)
58. L. Jinhai, M. Han, Y. Guo, F. Wang, L. Meng, D. Mao, S. Ding, C. Sun, Appl. Catal. A: Gen. **524**, 105 (2016)
59. L. Hou, H. Zhang, L. Wang, L. Chen, Chem. Eng. J. **229**, 577 (2013)
60. S. Liu, X.-R. Zhao, H.-Y. Sun, R.-P. Li, Y.-F. Fang, Y.-P. Huang, Chem. Eng. J. **231**, 441 (2013)
61. K. Saravanakumar, R. Karthik, S.M. Chen, J. Vinoth Kumar, K. Prakash, V. Muthuraj, J. Colloid Interf. Sci. **504**, 514 (2017)
62. F. Nekouei, S. Nekouei, Sci. Total Environ. **601–602**, 508 (2017)
63. H.R. Rajabi, F. Karimi, H. Kazemdehdashti, L. Kavoshi, J. Photochem. Photobiol., B **181**, 98 (2018)
64. H.R. Rajabi, M. Farsi, Mater. Sci. Semicond. Proc. **31**, 478 (2015)
65. M. Shamsipur, H.R. Rajabi, Spectrochim. Acta, Part A **122**, 260 (2014)
66. K. Saravanakumar, V. Muthuraj, Optik **131**, 754 (2017)
67. K. Saravanakumar, M.M. Ramjan, P. Suresh, V. Muthuraj, J. Alloys Compd. **664**, 149 (2016)
68. S. Khadtare, A.S. Bansode, V.L. Mathe, N.K. Shrestha, C. Bathula, S.-H. Han, H.M. Pathan, J. Alloys Compd. **724**, 348 (2017)
69. X. Zhang, X. Li, C. Shao, J. Li, M. Zhang, P. Zhang, K. Wang, N. Lu, Y. Liu, J. Hazard. Mater. **260**, 892 (2013)
70. C. Bi, J. Cao, H. Lina, Y. Wang, S. Chen, Appl. Catal. B: Environ. **195**, 132 (2016)
71. H. Park, H.-I. Kim, G.-H. Moon, W. Choi, Energy Environ. Sci. **9**, 411 (2016)
72. M. Pirhashemi, A. Habibi-Yangjeh, J. Colloid Interface Sci. **491**, 216 (2017)

Affiliations

Juan Cheng[1] · Xi Wang[1] · Zhenzong Zhang[1] · Yi Shen[1] · Kuan Chen[1] · Yongfu Guo[1] · Xiaoji Zhou[1] · Renbi Bai[1]

✉ Yongfu Guo
yongfuguo@163.com

✉ Renbi Bai
ceebairb@live.com

[1] Center for Separation and Purification Materials and Technologies, Suzhou University of Science and Technology, Suzhou 215009, Jiangsu, People's Republic of China